



# CHORUS

This is the accepted manuscript made available via CHORUS. The article has been published as:

## Migration mechanisms and diffusion barriers of carbon and native point defects in GaN

Alexandros Kyrtsos, Masahiko Matsubara, and Enrico Bellotti

Phys. Rev. B **93**, 245201 — Published 16 June 2016

DOI: [10.1103/PhysRevB.93.245201](https://doi.org/10.1103/PhysRevB.93.245201)

# Migration mechanisms and diffusion barriers of carbon and native point defects in GaN

Alexandros Kyrtsos,<sup>1</sup> Masahiko Matsubara,<sup>1</sup> and Enrico Bellotti<sup>1,2</sup>

<sup>1</sup>*Department of Electrical and Computer Engineering,  
Boston University, Boston, Massachusetts 02215, USA\**

<sup>2</sup>*Division of Materials Science and Engineering, Boston University, Boston, Massachusetts 02215, USA*

Carbon related defects are readily incorporated in GaN due to its abundance during growth both with MBE and MOCVD techniques. Employing first-principles calculations, we compute the migration barriers of carbon interstitials and we discuss possible relevant mechanisms of diffusion in the wurtzite GaN crystal. In addition, we calculate the migration barriers for the diffusion of the native defects of the crystal, i.e., gallium and nitrogen interstitials and vacancies. The Minimum Energy Path (MEP) and the migration barriers of these defects are obtained using the Nudged Elastic Band (NEB) method with the climbing image modification (CI-NEB). In addition, the Dimer method is used to independently determine the results. The results yield a quantitative description of carbon diffusion in GaN allowing for the determination of the most preferable migration paths.

## I. INTRODUCTION

III-Nitride semiconductors such as GaN have enabled the development of efficient LED lighting.<sup>1</sup> In addition to optoelectronic applications such as blue/green LEDs, GaN and its alloys are used in power electronics<sup>2</sup> as well as photovoltaic applications<sup>3</sup>. It is known that a high number of point<sup>4</sup> and extended<sup>5,6</sup> defects influence the electronic and optical properties of devices<sup>7,8</sup>. Defect related levels in the band gap may be the source of radiative recombination centers, leading to below gap emission which compromises the performance of the device. A typical example of such a level is centered around 2.2 – 2.3 eV and is often referred to as the yellow luminescence (YL)<sup>9–12</sup>. This YL band is present for both undoped samples<sup>13</sup> and samples containing carbon impurities.<sup>14–16</sup> Recent studies suggest that carbon related defects are responsible for the YL band.<sup>9,17</sup>

Carbon is a common impurity in GaN grown both with molecular beam epitaxy (MBE)<sup>18,19</sup> and metal organic chemical vapor deposition (MOCVD).<sup>20</sup> In the former case, carbon can contaminate the material during air exposure in standard substrate loading procedures or at the beginning of regrowth. In MOCVD, carbon is part of the metalorganic compounds used as source material for gallium. In addition, carbon can be found as a contaminant in the source gases or it is unintentionally released from the susceptor that transfers heat to the substrate. Furthermore, carbon is intentionally present as a dopant for resistive layers in devices.

Along with carbon, that can be found as a substitutional or interstitial impurity, native defects also play an important role in determining the electrical and optical properties of GaN. Furthermore, due to the potential applications of GaN as a radiation hard material,<sup>21</sup> understanding how these defects migrate under extreme operating conditions and determining their annealing temperatures is of primary importance for studying device reliability. In the present work, we propose the most probable mechanisms of carbon migration and we com-

pute the corresponding migration barriers. To investigate these phenomena we employ density functional theory (DFT)<sup>22,23</sup> in conjunction with the Climbing Image Nudged Elastic Band method (CI-NEB)<sup>24,25</sup> as well as the Dimer method.<sup>26</sup> In addition, using the same techniques, we study the most common native defects in GaN and we compute the migration barriers for charge states that have not been considered before. Previous theoretical results<sup>4,27,28</sup> are either incomplete or contradictory to our results. When available, we compare our results with experimental data.<sup>21,29–31</sup>

The NEB method provides a good representation of the diffusion path for a certain reaction. In fact, it finds a steepest descent (SD) path from saddle point(s) to minima.<sup>32</sup> In most cases, the SD path corresponds to the minimum energy path (MEP). The CI-NEB method not only provides information about the MEP, but also the transition state configuration at the saddle point. The NEB method is a chain-of-states method, i.e., a method in which several states of the system are connected together to trace out a path. This method may require a large number of images to successfully describe a diffusion path which is very computationally demanding for large systems. On the other hand, the Dimer method is a min-mode following method which allows to start from an initial configuration and search for nearby saddle points. One limitation of such a method is that when a local minimum is used as an initial configuration, it may converge to a saddle point that is irrelevant for the path of interest. Another is that it does not provide any information about the diffusion path. However, combining the two techniques enables one to achieve a good description of the reaction path and determine the saddle point. We employ the Dimer method to independently determine the migration barriers and compare with the results obtained by the CI-NEB.

The manuscript is organized as follows: In the following section (Section II), we present the details of the numerical model. In Section III we discuss the basic diffusion mechanisms in the wurtzite structure which are

relevant for the migration of split interstitials and substitutional defects. In Section IV we describe the results of our calculations for the native and the carbon related defects. We compare the basic mechanisms and we propose some possible interactions of carbon with native defects. In Section V we discuss the potential implications of the outcomes of our calculations. Section VI will conclude the manuscript.

## II. METHOD

The calculations were performed with the vienna *ab initio* simulation package (VASP)<sup>33</sup> using the projector augmented wave (PAW) method<sup>34,35</sup>. For the calculations of the migration barriers we used the generalized gradient approximation (GGA) in the parametrization by Perdew, Burke and Ernzerhof (PBE)<sup>36</sup> for the exchange-correlation functional. The formation energy calculations were performed using the Heyd-Scuseria-Ernzerhof (HSE) hybrid functional.<sup>37,38</sup> The investigation of the lowest energy paths and migration barriers was performed using the NEB<sup>24,25</sup> and the Dimer<sup>26</sup> methods as implemented in VASP through the VTST-Tools by Henkelman, Jónsson and others.<sup>39</sup>

The supercell of the wurtzite crystal can be constructed with either hexagonal or orthorhombic symmetry depending on the choice of the basis vectors. We performed calculations with supercells of 32, 64, 72, 96, 128, 144 and 192 atoms. The 32- and 72-atom supercells are hexagonal supercells while the rest are orthorhombic. In the case of the native defects, the smallest supercell we used was the 32-atom supercell, while for carbon the smallest was the 64-atom supercell. In both cases, we checked the convergence of our results using supercells of up to 192 atoms. Our reported values both for the native and the carbon related defects refer to the 96-atom supercell because it was found adequate to produce converged results compared to the larger supercells. The plane-wave basis energy cutoff was set at 450 eV and a  $\Gamma$ -centered  $2 \times 2 \times 2$   $k$ -point mesh was used for the sampling of the Brillouin zone resulting in 8 irreducible  $k$ -points. We also used a  $2 \times 2 \times 2$  Monkhorst-Pack mesh which results in 4 irreducible  $k$ -points and the results were similar to the  $\Gamma$ -centered mesh. The convergence of the basis-set as well as the  $k$ -points mesh was investigated using the 32-atom supercell in which a higher cutoff of 500 eV was used. In addition, a  $3 \times 3 \times 3$   $\Gamma$ -centered mesh was tested producing the same results with the  $2 \times 2 \times 2$  mesh. The atomic configurations were relaxed until the maximum force per atom was less than  $5 \times 10^{-3}$  eV/Å. In the case of the NEB and the Dimer calculations, the images were relaxed until the maximum force per atom was less than  $10^{-2}$  eV/Å and  $5 \times 10^{-3}$  eV/Å respectively.

The crystallographic parameters of the  $w$ -GaN we obtained from our calculations are  $a = 3.211$  Å,  $c/a = 1.629$  and  $u = 0.377$ , which are in good agreement with the experimental values of  $a = 3.189$  Å,  $c/a = 1.626$  and  $u =$

0.377 and consistent with previous DFT calculations.<sup>5,40</sup> The band gap at the  $\Gamma$  point is 1.76 eV which underestimates the experimental value of 3.4 eV. This was expected since the underestimation of the band gap is a known issue in standard DFT calculations using LDA or GGA.

We also carried out calculations for the formation energies of the native defects and the carbon interstitials using HSE. The same supercell size and  $k$ -point meshes were used. The energy cutoff was 425 eV and the convergence criterion for the relaxation was a maximum force per atom of less than 0.05 eV/Å. The amount of the exact exchange in the functional was 28% in order to reproduce the experimental band gap values and lattice constants. The full description of the formation energy calculations is available in Ref. [41].

The main sources of error in DFT calculations of point defects are the electrostatic and elastic interactions of the defects of neighboring supercells and the underestimation of the band gap. The former is due to supercell finite-size effects while the latter arises from the exchange-correlation functional. Lany and Zunger<sup>42</sup> describe a number of methods to overcome these shortcomings of standard DFT. In our case, we obtain the formation energies of the defects and their transition levels using HSE which does not suffer from the band gap error. We used the scheme proposed by Freysoldt *et al.*,<sup>43</sup> to account for the corrections in the formation energies of the charged defects. In the case of migration barriers, the main scope of the present work, the calculated values are obtained as differences between electronically similar configurations. Thus, finite-size effects corrections are not expected to play a significant role in the calculation of migration barriers. We applied the same correction scheme in some cases of charged defects and the differences were indeed small (less than 0.08 eV). Based on previous works,<sup>44,45</sup> a typical systematic error in the standard DFT formalism is considered to be of the order of 0.1 eV. Consequently, one should expect that the uncertainty of the migration barriers using standard DFT methods is at least of the same order.

In the NEB method,<sup>46</sup> a set of “images” of the system is used to represent the migration path from the initial to the final configuration. The images (i.e., atomic configurations along the migration path) are connected with springs to resemble a string (or band). An optimization algorithm is then applied to relax the string down towards the minimum energy path. In the climbing image modification, the highest energy image is driven to the saddle point by neutralizing the forces along the band. The highest energy image of the band corresponds to the saddle point and its energy difference compared to the initial states defines the migration barrier.

Since the CI-NEB method converges to the saddle point, one would expect that even using only one image, this image would represent the saddle point. Even though there are cases in which the path is trivial and the 1-image CI-NEB will give the correct result, in prac-

tice, it is always better to use a higher number of images. The number of images is an important parameter to consider in these calculations. Additional images increase dramatically the computational cost since the resources are shared among the images. Thus, it is important to achieve a balance between the good description of the minimum energy path and the number of images which minimize the computational cost. In our calculations, we used up to 16 images in some cases but most of our results are obtained with less than 10 images.

Our calculations involve an initial relaxation using the typical NEB method before proceeding with the modified CI-NEB. In addition, the Dimer method was used to independently determine the saddle point and the migration barrier. The Dimer method is useful in conjunction with the NEB because it can efficiently locate the saddle point after a few initial steps using the standard NEB method.

### III. DIFFUSION MECHANISMS

Starting from a nitrogen atom, there are three available paths for migration as shown in Fig. 1 and also discussed elsewhere.<sup>47</sup> Two of them are paths between first nearest neighbors on the nitrogen sublattice and the third is a path between two second nearest neighbors. Mechanism A corresponds to a jump between two first nearest neighbors which results in diffusion with components both parallel and perpendicular to the  $c$ -axis. Considering the four nitrogen atoms that establish a bond with a single gallium atom, three of them lie on a plane which is perpendicular to the  $[0001]$  direction ( $c$ -axis) and the fourth is out-of-plane. Mechanism A describes the migration of an atom forming a split with one of the three in-plane nitrogens to the fourth which is out-of-plane.

In the case of mechanism B, migration occurs between two adjacent nitrogens lying on a plane perpendicular to the  $[0001]$  direction. This mechanism is a first nearest neighbor migration jump and together with mechanism A is expected to exhibit the lowest migration barriers. Mechanism B is different from A in the manner that the diffusion is restricted in a plane perpendicular to the  $c$ -axis while mechanism A has components both parallel and perpendicular to the  $c$ -axis. Thus, mechanism B could cause anisotropy in the diffusion of a species since a certain direction is more preferable than others.

As an additional mechanism, we consider mechanism C which is a second nearest neighbor out-of-plane mechanism. Because this mechanism utilizes the hexagonal channel of the wurtzite structure, one might think that it allows for an easier path for the interstitial to move. However, our calculations show that moving through the hexagonal channel is energetically expensive and not a preferable path.

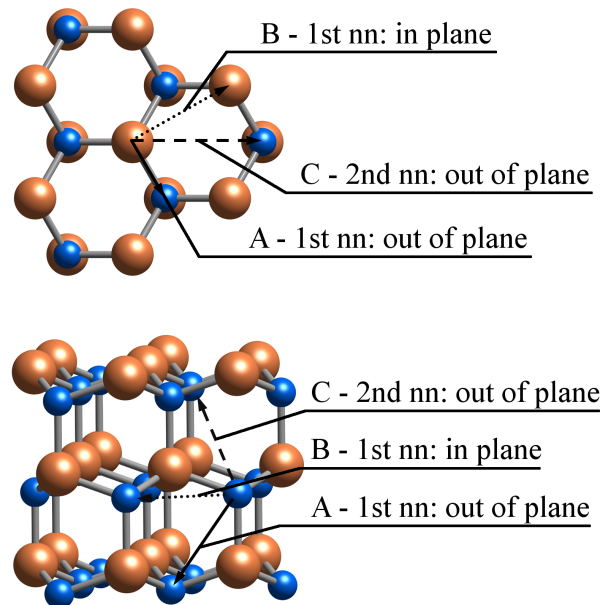


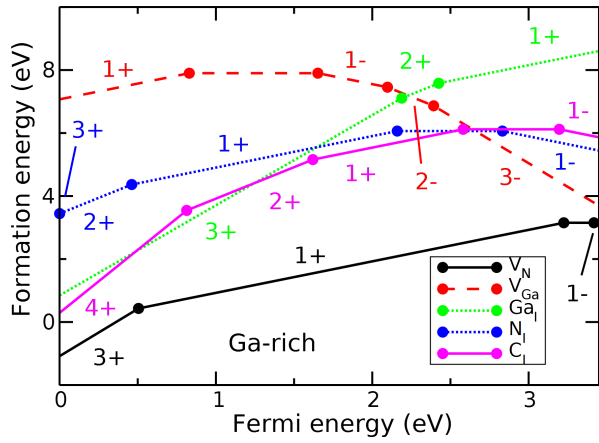
FIG. 1. Diffusion paths in the wurtzite structure considering jumps among the first and second nearest neighbors. Nitrogen atoms are represented as small blue spheres while gallium atoms are the large orange spheres.

## IV. RESULTS

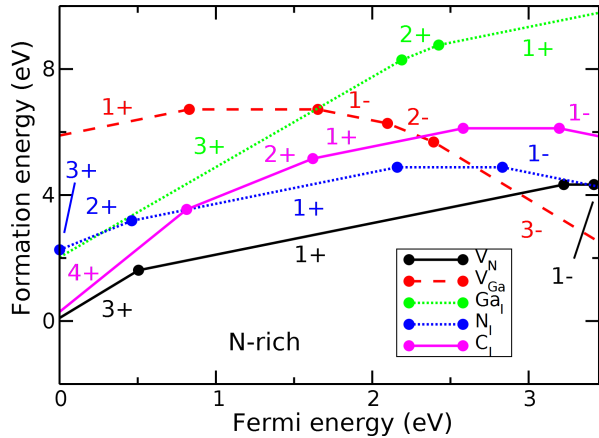
### A. Native defects

The native defects investigated in this work involve both the interstitials and the vacancies of nitrogen and gallium atoms in a number of different charge states. For completeness, we also consider charge states never previously reported. The formation energies of the interstitials are much higher compared to the vacancies,<sup>4</sup> however they can be created in non-equilibrium conditions such as irradiation. Using HSE calculations as described in Section II, we calculated the formation energies and the transition levels of the native defects as well as the carbon interstitials in both N- and Ga-rich conditions. The results are presented in Fig. 2.

In a previous work<sup>4</sup> the authors reported a calculated barrier value of 0.9 eV for the  $\text{Ga}_i^{3+}$  and mentioned that for the +2 and +1 charge states, the barriers should be slightly lower. Those calculations were performed using a method which relies on constraining the movement of the migrating atom. Based on detailed calculations we performed for the  $\text{Ga}_i^{3+}$  as well as the  $\text{Ga}_i^{2+}$  and  $\text{Ga}_i^{1+}$ , we found that the migration barriers for +2 and +1 are higher than the one for +3. Furthermore, for the nitrogen interstitial and the vacancies, the authors reported only the results for mechanism A. However, our calculations indicate that in many cases mechanism B exhibits a lower barrier. We also compare our results with experimental data when available. In the following sections we present the results of the native defects in detail. Table I



(a) Formation energies of the native defects and the carbon interstitials in Ga-rich conditions.



(b) Formation energies of the native defects and the carbon interstitials in N-rich conditions.

FIG. 2. Formation energies of the native defects and the carbon interstitials obtained using the HSE hybrid functional for Ga- and N-rich conditions.

summarizes our results using the 96-atom supercell and only the value of the most favorable mechanism is shown in each case.

### 1. Nitrogen interstitial $N_i$

The migration of  $N_i$  in mechanism A proceeds as presented in Fig. 3 through an interstitialcy mechanism. Initially, the split consists of atoms N1 and N2 while N3 occupies the usual site for nitrogen in the wurtzite crystal. The migrating atom in this case is N2 but both N1 and N2 move upwards until N2 forms a new split with N3. In the case of mechanism B, N2 would move in a plane perpendicular to the  $c$ -axis. Both mechanisms A and B are investigated for charge states ranging from  $-1$  to  $+3$  using a 96-atom supercell. We also studied mechanism A in the aforementioned charge states using the 32-atom supercell in order to have a direct comparison to previous results.<sup>4</sup>

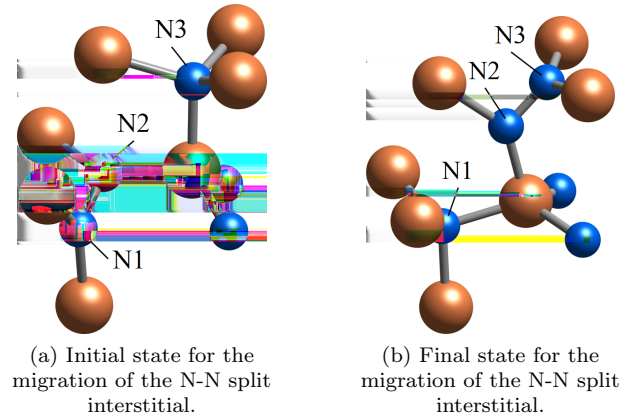


FIG. 3. Initial and final states of the nitrogen interstitial migration.

In the case of the 32-atom supercell, the lowest migration barrier is observed at a value of 1.5 eV for the  $N_i^{1-}$ , while the highest barrier corresponds to the neutral interstitial at 2.3 eV. The calculated values for  $N_i^{1+}$ ,  $N_i^{2+}$  and  $N_i^{3+}$  are 2.1, 2.0 and 1.6 eV respectively. Our results are in good agreement with a previous theoretical work in the 32-atom supercell,<sup>4</sup> as well as other supercell sizes.<sup>27,28</sup> The most notable difference is the case of  $N_i^{2+}$  where our calculated value of 2.0 eV differs from the previously reported value of 2.5 eV.<sup>4</sup> There is evidence that the migration barriers may be different depending on whether the calculation was performed under the LDA (used in Ref. [4]) or the GGA formalism.<sup>48</sup> However, if the migration barrier of  $N_i$  was subject to the type of the functional used, one would expect significant differences in all the charge states. Hence, we attribute this discrepancy to the difference of the method used in this work.

In the case of the 96-atom supercell, we performed calculations both for mechanism A and B. The calculated values of the migration barriers in mechanism A are 1.9, 2.4, 2.2, 2.1 and 2.1 eV in the charge states ranging from  $-1$  to  $+3$  respectively. The corresponding values for mechanism B are 1.9, 2.4, 2.1, 2.2 and 1.7 eV. Calculations in larger supercells show that the 96-atom supercell produces converged results within 0.05 eV.

The energy barriers for mechanism A using the 96-atom supercell are in good agreement with the ones calculated using the 32-atom supercell except for the  $N_i^{1-}$  and  $N_i^{3+}$  for which the energy barrier is 0.4 and 0.5 eV higher respectively. This indicated that the 32-atom supercell is not large enough to model these defects. In fact, the larger supercell makes it possible to account for the larger deformation that occurs during the migration of the  $N_i^{3+}$ . We would like to note that in all cases except for  $N_i^{3+}$ , both mechanisms exhibit either the same or slightly different barrier but in the case of  $N_i^{3+}$  there is a clear preference for mechanism B.

Electron paramagnetic resonance measurements<sup>21</sup> indicate that  $N_i$  anneals at 670 K. This annealing temperature indicates a migration barrier of approximately

1.7 eV. Also, the authors most likely observe the  $N_i^{1-}$ . Hence our calculated value of 1.9 eV is in good agreement with their experimental results.

## 2. Gallium interstitial $Ga_i$

Our HSE calculations (Fig. 2) show that the stable charge states for  $Ga_i$  range from +3 to +1. It has been shown before that the  $Ga_i$  favors a site near the octahedral ( $O$ ) site in the center of the hexagonal channel as presented in Fig. 4a. Apart from the  $O$ -site, the  $A$ -site has been discussed in the past and was considered to be a local minimum.<sup>4,49,50</sup> In the cases of  $Ga_i^{3+}$  and  $Ga_i^{2+}$  the  $O$ -site is found to exhibit the lowest energy according to our calculations. However, it is just a local minimum in the case of  $Ga_i^{1+}$ . In fact,  $Ga_i^{1+}$  relaxes to a different site which is neither the  $A$  nor the  $O$ -site. We will refer to this as  $A'$ -site. Fig. 4 shows the two stable configurations for the  $Ga_i$ . To the best of our knowledge, this is the first time the  $A'$ -site is reported as a global minimum for the  $Ga_i^{1+}$ . Our HSE calculation confirms the existence of the  $A'$ -site as a global minimum.

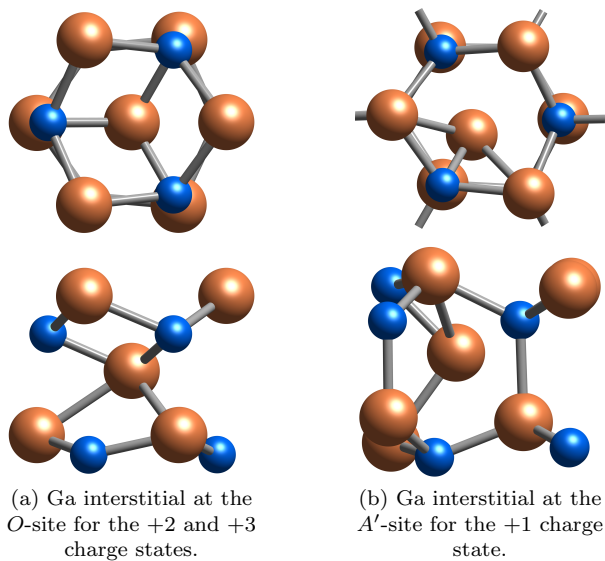


FIG. 4. Top and side view of Ga interstitial in the +1, +2 and +3 charge states.

The migration path of the  $Ga_i$  involves movement both parallel and perpendicular to the  $c$ -axis. The atom located at the  $O/A'$ -site pushes one of the neighboring gallium atoms to an interstitial site while the former relaxes in the latter's initial position. Thus, gallium migrates via an interstitialcy mechanism. The lowest barrier is observed for the +3 charge state at 0.7 eV. Experimental results<sup>51</sup> suggest that gallium interstitials are mobile even at room temperatures which is in good agreement with our results.

Adding electrons to the system increases the migration barrier to 1.1 and 1.6 eV (Fig. 5) for the +2 and +1

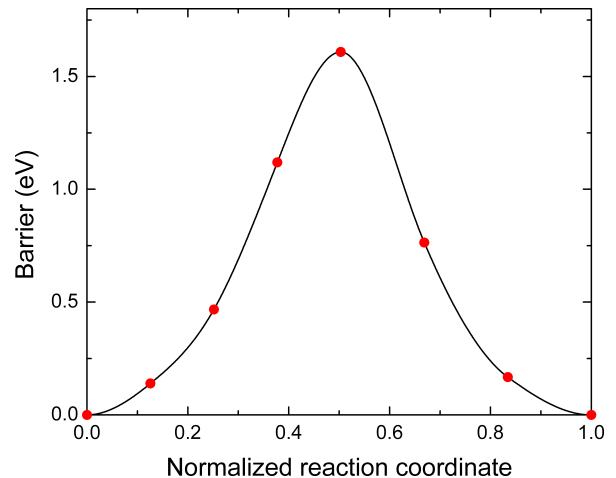


FIG. 5. Migration barrier of the  $Ga_i^{1+}$  using six images.

charge states respectively. The  $Ga_i^{1+}$  resides closer to its neighboring gallium atoms compared to the other two charge states. In the saddle point, however, the distance between the two atoms involved in the migration is the largest for the +1 charge. This causes a large deformation of the crystal structure at the saddle point configuration which results in a higher migration barrier.

## 3. Nitrogen vacancy $V_N$

Nitrogen vacancies exhibit low formation energies, especially for  $p$ -type GaN and they have been claimed to be the major point defects in GaN.<sup>27</sup> The most stable charge states under the PBE formalism are the single and triple positively charged nitrogen vacancies. However, using hybrid functionals (HSE), we calculated that the neutral and the  $-1$  charge states also appear in the band gap (Fig. 2) in the  $n$ -type region.<sup>41,52</sup> We examined both in-plane (mechanism A, Fig. 1) and out-of-plane (mechanism B, Fig. 1) migrations of the  $V_N$  between adjacent first nearest neighbor sites for the above mentioned charge states.

The  $V_N^{3+}$  exhibits the same migration barrier both for in-plane and out-of-plane migrations at 2.7 eV. In the other three charge states, i.e., +1, neutral and  $-1$ , there is a clear preference towards mechanism B. In the case of  $V_N^{1+}$ , the results for mechanism A and B are 3.8 and 4.1 eV respectively. Both results are in very good agreement with the experimental result of Ambacher *et al.*,<sup>29</sup> who estimated the migration barrier to be  $4.1 \pm 0.4$  eV. The barrier for mechanism A in the case of neutral  $V_N$  and  $V_N^{1-}$  is 3.4 and 2.6 eV respectively. Regarding mechanism B, the barriers are 2.7 and 2.0 eV for neutral  $V_N$  and  $V_N^{1-}$  respectively showing a clear preference over mechanism A.

TABLE I. Migration energy barriers for native defects obtained by CI-NEB calculations. Only the most preferable mechanism is shown (in the parentheses) in each case. An asterisk denotes a charge state that is not predicted by PBE.

Defect	Charge state	Barrier (eV) <sup>a</sup>	Barrier (eV) <sup>b</sup>
$\text{Ga}_i$	+3	0.7	0.9
	+2*	1.1	$\leq 0.9$
	+1*	1.6	$\leq 0.9$
$\text{N}_i$	+3	1.7 (B)	1.4
	+2	2.1 (A)	2.5
	+1	2.1 (B)	2.1
	0	2.4	2.4
	-1	1.9	1.6
$V_{\text{N}}$	+3	2.7	2.6
	+1	3.8 (B)	4.3
	0*	2.7 (B)	
	-1*	2.0 (B)	
$V_{\text{Ga}}$	-3	2.1 (A)	1.9
	-2	1.9 (A)	
	-1	1.5 (B)	
	0	2.5 (B)	

<sup>a</sup>The present work.

<sup>b</sup>Ref. [4]

#### 4. Gallium vacancy $V_{\text{Ga}}$

Gallium vacancies are relevant for  $n$ -type material because they exhibit the lowest formation energy for  $V_{\text{Ga}}^{3-}$ . However, we consider all the charge states from  $-3$  to the neutral case in order to account for all the different Fermi levels. We calculated the migration barrier for both in-plane and out-of-plane migration taking into account only first nearest neighbor jumps.

Our calculations show only a minute difference between the in-plane and out-of-plane migration of  $V_{\text{Ga}}^{3-}$ . The former has a barrier of 2.2 eV while the latter has a barrier of 2.1 eV. These results are in good agreement with previous experimental results.<sup>53</sup> In the case of  $V_{\text{Ga}}^{2-}$  we observe a difference for the two different orientations. The energy barrier for the in-plane diffusion corresponds to 1.9 eV while the out-of-plane diffusion has a much larger barrier at 2.3 eV. The same is true for the  $V_{\text{Ga}}^{1-}$  as well. In fact, in the case of  $V_{\text{Ga}}^{1-}$  the difference is even more profound since the out-of-plane barrier is 2.5 eV while the in-plane barrier is just 1.5 eV. The neutral vacancy which is also the least probable, exhibits high migration barriers at 2.5 and 2.8 eV for in-plane and out-of-plane migration respectively.

#### B. Carbon related defects

The carbon related defects we investigated involve mainly carbon interstitials. Even though carbon com-

plexes are also important for the electronic properties of GaN, they are not investigated in this work. Using the initial configurations discussed elsewhere<sup>41,54</sup> as possible interstitial sites, we let the structures relax. Our calculations show that there are four different relevant configurations for the carbon interstitial. One of them is the channel configuration shown in Fig. 6d where the carbon resides near the center of the  $c$ -axis channel and the rest are split interstitials with a nitrogen atom. For brevity, we refer to the type-1, type-2 and type-3 splits as  $s_1$ ,  $s_2$  and  $s_3$  respectively. As presented in Fig. 2, the relevant charge states for  $\text{C}_i$  vary from  $+4$  to  $-1$  except for the triple positively charged defect. In all cases a split interstitial is found to be the most stable configuration except for the  $\text{C}_i^{4+}$  which resides at the channel site.

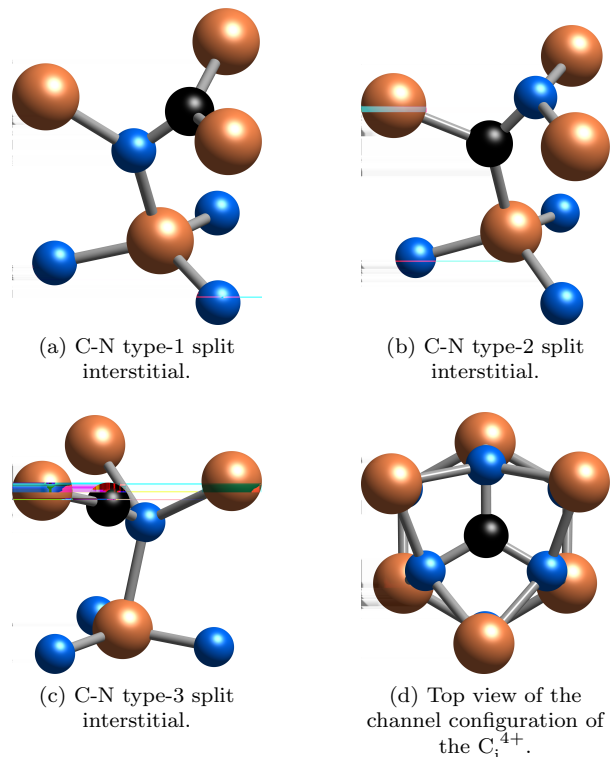


FIG. 6. Different types of split interstitials between carbon (black) and nitrogen (blue) atoms.

In the case of the neutral  $\text{C}_i$ , the two most stable configurations are the  $s_1$  and  $s_2$  C-N split complexes shown in Fig. 6. Our calculations as well as previously reported results<sup>41,54</sup> show that the two types differ by less than 0.1 eV for the neutral  $\text{C}_i$ . The same configurations are stable for  $\text{C}_i^{1+}$  and  $\text{C}_i^{1-}$  as well. In the former, the energy difference is small, while in the latter the difference is almost 0.2 eV. In the case of  $\text{C}_i^{2+}$ ,  $s_2$  and  $s_3$  are the most stable. Since the two most stable configurations are so close energetically, we investigate both as potential initial and final configurations for the diffusion of carbon. In other words, the migration mechanisms we investigated are not limited to diffusion among the most stable configurations, but among local minima as well.

The small energy difference and the similarity of the two configurations allows for migrations accompanied by transformation from one type to the other. For instance, the initial state of a reaction might be a  $s_2$  interstitial while the final state might be a  $s_1$  even though the latter might be just a local minimum. In this case, the migration barrier is not the same for both directions of the reaction because starting from the configuration with the higher formation energy the barrier is lower. We define the migration barrier as the energy difference between the saddle point and the lowest energy configuration. As a result, we report the barrier which is larger between the two directions in cases where the initial and the final states are different.

For the migration paths investigated for the carbon related defects we use the same terminology as in the native defects and as shown in Fig. 1. These paths are relevant only when the stable configurations are either one of the three interstitial types or a substitutional atom. Every split has three equivalent orientations at a given lattice site. Carbon is a foreign atom in GaN and the orientation as well as the type of the split are important for the diffusion of carbon interstitials. In many cases reorientation of the split is possible between consecutive jumps. We summarize our results for the carbon interstitials in Table II.

### 1. Carbon interstitials

We first examine the case of the neutral carbon interstitial where the two most stable configurations are  $s_1$  and  $s_2$ . The difference in the formation energy between the two types of interstitials is 0.1 eV with  $s_2$  being the lower in energy. The bond length between the carbon and the nitrogen is 1.29 Å and 1.31 Å for  $s_1$  and  $s_2$  respectively which are in excellent agreement with hybrid functional calculations.<sup>41</sup> The lowest migration barrier is obtained for the case of mechanism A from  $s_2$  to  $s_1$ . This barrier becomes even smaller by approximately 0.1 eV if the direction of the reaction is reversed. The diffusion potential energy along the reaction path is shown in Fig. 7. Most of the first nearest neighbor in-plane migrations (mechanism B) exhibit barriers close to 3 eV making them unfavorable compared to their out-of-plane counterparts (mechanism A). As expected, second nearest neighbor out-of-plane migrations (mechanism C) require a much greater energy. According to our calculations, the migration barrier for a mechanism C migration is 4 eV. Such a high barrier results in an extremely unfavorable path.

Focusing only on mechanisms A and B, it is obvious that the most favorable path involves a  $s_1/s_2$  transformation. This is not surprising since the path in this case is very short and the orientation of the atoms is favorable. In the case of a  $s_2/s_2$  migration the barrier is 2.6 eV while it is 0.1 eV lower for a  $s_1/s_1$  migration. In the case of mechanism B, we obtained a barrier of 2.5 eV for a

jump between two  $s_1$  sites. Even though  $s_1$  is not the most stable interstitial energetically, it exhibits a much lower barrier than the other two jumps of this mechanism. Hence, it is expected to play an important role in the migration of the neutral  $C_i$ .

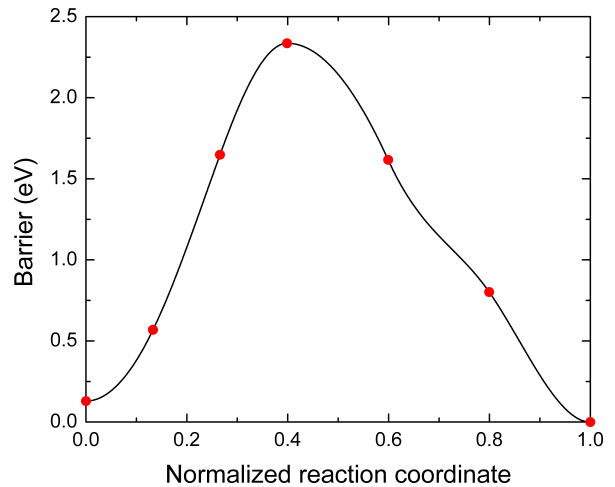


FIG. 7. Migration energy barrier for a mechanism A jump from a type-1 to a type-2 carbon interstitial in the neutral case using five images.

The two most stable states for  $C_i^{1+}$  are the  $s_1$  and  $s_2$  interstitials as in the neutral case. However, their difference in this case is within 0.05 eV. As a result, we consider both  $s_1$  and  $s_2$  as equally probable configurations for  $C_i^{1+}$ . The bond length between the carbon and the nitrogen is 1.24 Å in both  $s_1$  and  $s_2$ . The two structures are very similar with respect to the positions of the atoms with the only difference being that carbon and nitrogen interchange sites. The calculated value in most cases is 2.6 eV. For the jump between two  $s_1$  sites in mechanism B the barrier is calculated at 2.4 eV. We also consider the jump between second nearest neighbors but the barrier is more than 4 eV so it is too high to play any role in the diffusion of  $C_i^{1+}$ .

As in the two previously discussed charge states,  $s_1$  and  $s_2$  are the most important configurations for  $C_i^{1-}$ . The formation energy of  $s_2$  is 0.2 eV lower than  $s_1$  which is enough for  $s_1$  to be considered unfavorable but even in this case we investigate them both. The bond length between the carbon and the nitrogen is 1.35 Å and 1.37 Å for  $s_1$  and  $s_2$  respectively. Mechanism A is slightly more favorable than mechanism B for this charge state. The barrier is 2.9 eV in the case of mechanism A and 3.0 eV in the case of mechanism B. Our results for the C mechanism in other charge states indicate that this is a very unfavorable jump compared to A and B so we did not perform any calculations in this case.

The last split interstitial we investigated is the double positively charged  $C_i^{2+}$ . The two most stable configurations in this case are  $s_2$  and  $s_3$  with  $s_3$  being lower than  $s_2$  for less than 0.1 eV. Removing two electrons from the system causes the nitrogen-carbon bond to become



TABLE II. Energy barriers for carbon interstitial migration as obtained from CI-NEB calculations. In all cases except for the  $C_i^{2+}$ ,  $s_i/s_j$  refers to  $s_1/s_2$ . In the case of  $C_i^{2+}$  the type-1 split is replaced by the type-3 and  $s_i/s_j$  refers to  $s_3/s_2$ . An asterisk denotes a charge state that is not predicted by PBE.

Migration Mechanism	Initial/Final	Barrier (eV)			
		$q = -1^*$	$q = 0^*$	$q = +1$	$q = +2$
A	$s_i/s_i$		2.5	2.6	2.0
	$s_j/s_j$	2.9	2.6	2.6	2.0
	$s_i/s_j$	2.9	2.3	2.6	2.0
B	$s_i/s_i$	2.8	2.5	2.4	1.8
	$s_j/s_j$	3.0	3.0	2.6	1.6
	$s_i/s_j$	3.0	3.0	2.6	1.6
C	$s_i/s_i$		4.0	4.4	
	$s_j/s_j$				
	$s_i/s_j$		4.0	4.3	

even shorter at 1.184 Å for both  $s_2$  and  $s_3$  and also produces large outwards relaxations of the surrounding gallium atoms. The migration barrier of  $C_i^{2+}$  is the lowest of all cases. Specifically, mechanism B is the prevalent mechanism with barriers of 1.8 and 1.6 eV. Mechanism A exhibits slightly higher barrier at 2.0 eV.

The  $C_i^{4+}$  is different than the other charge states we investigated in the sense that it adopts the channel configurations shown in Fig. 6d instead of a split interstitial. The carbon atom resides in the center of the equilateral triangle of side 2.4 Å formed by the surrounding nitrogens.<sup>55</sup>

The migration along the hexagonal channel is the obvious path one would look at first. However, our calculations indicate that diffusion is not favored inside the channel. Instead, the carbon atom slides along the channel walls passing through local minima. Our calculations could not converge to a single step jump from the initial to the final state. Instead, the carbon atom was passing through several local minima indicating that this is not a single step process. According to our calculations, the individual steps along the path require less than 2 eV.

## 2. Carbon substitutionals and rotations

In order to have a better insight of carbon diffusion in GaN we also study two additional mechanisms. First, we investigate the interaction of carbon related defects with nitrogen interstitials and vacancies. In the case of the nitrogen interstitials, a  $N_i$  and a  $C_N$  could cause the creation of a  $C_i$ . It is expected that a vacancy in the vicinity of the carbon interstitial could result in the filling of the vacancy by either the nitrogen or the carbon. Another consideration originates from the fact that there are three equivalent orientations for a given split at a given lattice site. We studied the energy required to change the orientation of the split. In addition to the change in the orientation, we also examined the change of type. In general, we will refer to these reactions as rotations. Ro-

tations are important if a jump is divided in a two step process. For instance, a  $s_2/s_2$  jump in mechanism A can be divided in a two step process as a  $s_2/s_1$  rotation and a  $s_1/s_2$  jump. In the case of native defects, the migrating atoms are indistinguishable. Unlike native defects, carbon is a foreign species and the orientation of the split plays an important role in the overall diffusion process.

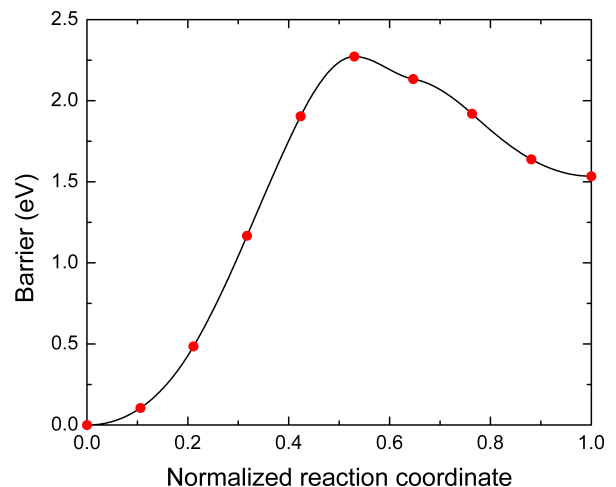


FIG. 8. Migration barrier for the migration of nitrogen from the C–N split pair to form a  $C_N$  and a  $N_i$ .

The initial state in Fig. 8 is the  $s_2$  neutral split. The nitrogen from the C–N split pair jumps using mechanism A to create a nitrogen split interstitial. The carbon remains in the nitrogen site as substitutional ( $C_N$ ). The energy required for such a process is 2.3 eV which is the same as in the case of the migration of carbon. The same mechanism was also investigated for the +1 charge state where the barrier was calculated to be 3.0 eV. Starting from a neutral system of a  $s_1$  interstitial and a vacancy, we calculated the migration barrier of filling the vacancy with the carbon using mechanism A. Our value for this process is 0.8 eV which is very low as expected.

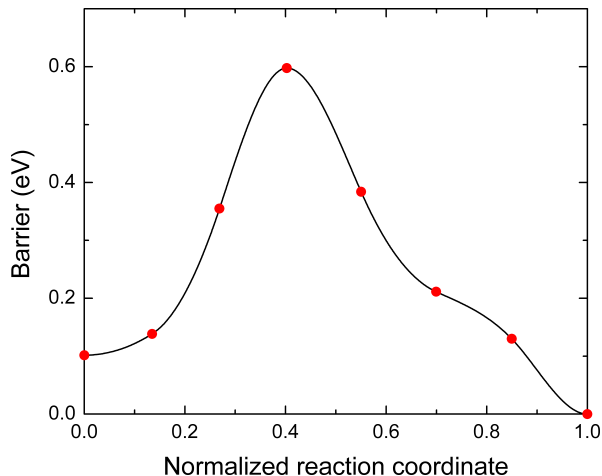


FIG. 9. Rotation from type-1 to type-2 for the neutral carbon interstitial.

In the neutral charge state, we examine the rotations  $s_1/s_1$ ,  $s_2/s_2$  and  $s_1/s_2$ . The barriers for such processes are 0.3, 0.4 and 0.6 eV (Fig. 9) respectively. The barrier for a  $s_1/s_2$  rotation at the +1 charge state is 0.4 eV. Given such low barriers, these mechanisms are active at temperatures close to 170 K, which is much lower than the temperature where actual diffusion of carbon occurs. In addition, their low barriers indicate that rotations can be easily combined with the main jumps.

## V. DISCUSSION

As discussed in the previous sections, we used the PBE exchange correlation functional to study the diffusion of native and carbon related defects. However, some charge states that are predicted to be stable by HSE do not appear in PBE calculations unless band gap correction is artificially introduced. Typical examples of such states are the  $C_i^{1-}$  and  $Ga_i^{1+}$  which are stable in the band gap in HSE, as shown in Fig. 2. We performed the corresponding calculations keeping in mind that these results might have more ambiguity.

In some of the paths we studied, the saddle point remained the same even though the initial and final states were different. This would normally indicate that the calculated saddle point is not a first order saddle point. In the case of a first order saddle point, all the modes or eigenvalues of the Hessian matrix should be positive except one. The negative eigenvalue points towards the direction of the reaction path. If there is more than one negative eigenvalue, the saddle point is of higher order meaning that there are multiple paths leading to the same transition state. In cases where the saddle point happens to be the same, we carefully examined the path followed by the migrating atom. As described in the previous section, a rotation takes place before the main jump which leads to the same saddle point. In addition,

we performed vibrational frequencies calculations for the transition state to examine the order of the saddle points. In all cases only one negative eigenvalue was found confirming that the saddle points are first order.

Even though the reaction rates are beyond the scope of this paper, we would like to highlight Quapp's work<sup>56</sup> where he addresses the case in which two reactions have the same saddle point. The branching of the path may occur in the presence of a ridge bifurcation in the potential energy surface. If the branching occurs before the transition state, there will be a separate saddle point for each branch leading to different products. In this case, transition state theory can be used to estimate the relative rates.<sup>57</sup> However, if the branching occurs after the saddle point, transition state theory cannot be used. The mechanisms we observed in our calculations are neither of these cases. Instead, jumps which share the same saddle point involve an initial rotation.

It is empirically observed that most diffusion processes in solids exhibit a temperature dependence described by an Arrhenius law of the form

$$D = D_0 e^{-\frac{Q}{k_B T}}, \quad (1)$$

where  $D$  is the diffusivity,  $D_0$  is a temperature independent factor,  $Q$  is the activation energy for the atomic jump mechanism and  $k_B T$  is the product of the Boltzmann constant with temperature. The activation energy,  $Q$ , is given as the sum of the formation energy and the migration barrier. Deviations from this equation may be caused by the existence of short circuiting diffusion paths such as dislocations and grain boundaries, multiple diffusion mechanisms and other impurity effects.<sup>58</sup> A derivation of the diffusivities for wurtzite crystals can be found in the work by Erhart and Albe.<sup>47</sup>

In order to estimate the annealing temperatures based on the migration barriers derived by our calculations, we used the Harmonic Transition State Theory (HTST). Within HTST, the potential energy near the stable sites of atoms is considered to be approximated by a second order energy expansion. In other words, the vibrational modes are harmonic. In addition, the modes perpendicular to the reaction coordinate at the saddle point are also considered to be harmonic. The HTST is a classical theory and cannot capture any quantum or any anharmonic effects. However, for the purposes of this work the HTST framework is used as a first order approximation to roughly estimate the temperatures at which the defects are mobile. Using HTST, the rate of a reaction is given as<sup>59-62</sup>

$$\begin{aligned} \Gamma^{\text{HTST}} &= \frac{\prod_i^{3N} \nu_i^{\min}}{\prod_i^{3N-1} \nu_i^{\text{saddle}}} e^{-\frac{E_b}{k_B T}} \\ &= \Gamma_0 e^{-\frac{E_b}{k_B T}}. \end{aligned} \quad (2)$$

Here  $E_b$  is the static barrier height (i.e.,  $T = 0$ ). In the preexponential factor,  $\nu_i^{\text{min}}$  are the  $3N$  normal mode frequencies at the stable site and  $\nu_i^{\text{saddle}}$  are the  $3N - 1$  non-imaginary normal mode frequencies at the saddle point. Usually this prefactor is in the range of  $10^{12} - 10^{13}$  Hz and eq. (2) should be used to rigorously calculate the attempt frequency  $\Gamma_0$ . However, as an approximation, the Einstein or the Debye frequency is often used instead. The only temperature dependence in eq. (2) is in the exponential. Using this formalism, the entropic effects are incorporated in the prefactor.

With regard to the temperature where carbon interstitials are mobile we assume a jump rate of 1 Hz and a typical Debye frequency of 10 THz. Then, using eq. (2) and the calculated migration barriers, one can estimate the annealing temperature. Hence, using  $\Gamma = 1$  Hz,  $\Gamma_0 = 10^{13}$  Hz and  $E_b = 2.3$  eV we estimate that carbon interstitials become active at temperatures close to 890 K. These temperatures are relevant during growth of GaN both with MBE and MOCVD techniques. In the case of  $C_i^{2+}$ , carbon could be mobile at even lower temperatures of approximately 660 K.

For charged point defects, the migration barrier may be lowered by applying an electric field along the direction of migration. Assuming that the charge is localized close to the defect, the barrier lowering is given by<sup>28</sup>

$$\Delta E = \mathcal{E}ql, \quad (3)$$

where  $\mathcal{E}$  is the electric field along the direction of migration,  $q$  is the charge of the defect and  $l$  is the distance between the initial state and the saddle point. Typically this distance is of the order of a few angstroms. In power electronics devices, fields may reach values of 3 MV/cm. The barrier drops by 0.2 eV in this case for a doubly charged defect. Even in high electric fields, the barrier lowering is not enough to activate carbon at room temperatures but it greatly enhances the diffusion.

It has been proven that optical excitation enhances the migration of interstitial Ga.<sup>31</sup> Except for an Auger process, nonradiative recombination at a deep trap may be accompanied by the release of a large amount of vibrational energy in the vicinity of the defect. In general, wide band-gap semiconductors are favored by recombination-enhanced defect reactions, especially in the case of deep trap levels<sup>63</sup> since the energy converted to vibrational energy is comparable to the migration barrier. Carbon interstitials are considered deep trap levels and their levels are comparable to the migration barriers. As a result, we speculate that interstitial carbon may be greatly affected by such phenomena.

## VI. CONCLUSIONS

We employed the Climbing Image Nudged Elastic Band method to explore migration barriers of native and carbon related defects in GaN. We studied the most relevant charge states of the above mentioned defects and

we propose mechanisms for the diffusion of carbon. The Dimer method was also used as a complementary method in order to compare with the results obtained by the CI-NEB. The two most stable interstitial types of carbon at each charge state were investigated with respect to diffusion via first and second nearest neighbor mechanisms.

Regarding our native defects results, they are in good agreement with the available experimental data. The  $Ga_i$  exhibits the lowest barrier among all the native defects. We have also shown that each charge state has a different preferable mechanism of diffusion but most of them exhibit lower barriers in the case of mechanism B. This result contradicts the previous notion that mechanism A was the most preferable.

In the case of carbon, the first nearest neighbor out-of-plane mechanism exhibits the lowest migration barriers in the neutral and +1 charge states. In the -1 charge state, in-plane and out-of-plane mechanisms are comparable while in the +2 charge state in-plane diffusion is more favorable. However, at growth temperatures, both mechanisms are expected to be present. Migration via the second nearest neighbor mechanism exhibits high energy barriers minimizing the probability for this mechanism to contribute to the carbon diffusion.

Our calculations for the secondary mechanisms show that transformations from one type of interstitial to the other can occur at very low temperatures. Since carbon is a foreign atom in GaN, the orientation of the interstitial is important in the diffusion process. Thus, these mechanisms are expected to play a significant role in the migration of carbon. In addition, we presented two possible interactions of carbon interstitials with nitrogen interstitials and vacancies.

Finally, we used the Harmonic Transition State Theory to roughly estimate the annealing temperatures of the native and the carbon related defects. Based on the calculated migration barriers, the native defects are expected to anneal at temperatures above 600 K. However, the  $Ga_i$  is expected to be mobile even at room temperatures due to its very low migration barrier. Carbon related defects exhibit higher barriers and are expected to anneal at temperatures of roughly 900 K which are relevant for growth of GaN both in MBE and MOCVD techniques.

## ACKNOWLEDGMENTS

We acknowledge useful and fruitful discussions with D. Coker, L. Pizzagalli, S. Sharifzadeh, and B. C. Rinderpacher. The authors gratefully acknowledge financial support from the U.S. Army Research Laboratory through the Collaborative Research Alliance (CRA) for Multi-Scale multidisciplinary Modeling of Electronic Materials (MSME). The computational resources were provided by the 2014 ARO DURIP Award made to Dr. E. Bellotti and the DoD HPC Open Research Systems.

- \* Electronic address: akyrtsos@bu.edu
- <sup>1</sup> S. Pimputkar, J. S. Speck, S. P. DenBaars, and S. Nakamura, *Nature Photonics* **3**, 180 (2009).
  - <sup>2</sup> U. K. Mishra, P. Parikh, and Y. F. Wu, *Proceedings of the IEEE* **90**, 1022 (2002).
  - <sup>3</sup> R. Dahal, J. Li, K. Aryal, J. Y. Lin, and H. X. Jiang, *Applied Physics Letters* **97**, 1 (2010).
  - <sup>4</sup> S. Limpijumnong and C. G. Van de Walle, *Phys. Rev. B* **69**, 035207 (2004).
  - <sup>5</sup> M. Matsubara, J. Godet, L. Pizzagalli, and E. Bellotti, *Applied Physics Letters* **103**, 262107 (2013).
  - <sup>6</sup> M. Matsubara, L. Pizzagalli, and E. Bellotti, *physica status solidi (c)* **11**, 521 (2014).
  - <sup>7</sup> C. G. Van De Walle and J. Neugebauer, *Journal of Applied Physics* **95**, 3851 (2004).
  - <sup>8</sup> F. Tuomisto, T. Paskova, S. Figge, D. Hommel, and B. Monemar, *Journal of Crystal Growth* **300**, 251 (2007).
  - <sup>9</sup> D. O. Demchenko, I. C. Diallo, and M. A. Reshchikov, *Phys. Rev. Lett.* **110**, 087404 (2013).
  - <sup>10</sup> T. Suski, P. Perlin, H. Teisseyre, M. Leszczynski, I. Grzegory, J. Jun, M. Bockowski, S. Porowski, and T. D. Moustakas, *Applied Physics Letters* **67**, 2188 (1995).
  - <sup>11</sup> M. A. Reshchikov and H. Morkoç, *Journal of Applied Physics* **97** (2005), 10.1063/1.1868059.
  - <sup>12</sup> T. Ogino and M. Aoki, *Japanese Journal of Applied Physics* **19**, 2395 (1980).
  - <sup>13</sup> E. R. Glaser, T. A. Kennedy, K. Doverspike, L. B. Rowland, D. K. Gaskill, J. A. Freitas, M. Asif Khan, D. T. Olson, J. N. Kuznia, and D. K. Wickenden, *Phys. Rev. B* **51**, 13326 (1995).
  - <sup>14</sup> S. O. Kucheyev, M. Toth, M. R. Phillips, J. S. Williams, C. Jagadish, and G. Li, *Journal of Applied Physics* **91**, 5867 (2002).
  - <sup>15</sup> C. H. Seager, A. F. Wright, J. Yu, and W. Götz, *Journal of Applied Physics* **92**, 6553 (2002).
  - <sup>16</sup> A. Armstrong, A. R. Arehart, D. Green, U. K. Mishra, J. S. Speck, and S. A. Ringel, *Journal of Applied Physics* **98** (2005).
  - <sup>17</sup> J. L. Lyons, A. Janotti, and C. G. Van De Walle, *Applied Physics Letters* **97**, 5 (2010).
  - <sup>18</sup> G. Koblmüller, R. M. Chu, A. Raman, U. K. Mishra, and J. S. Speck, *Journal of Applied Physics* **107** (2010).
  - <sup>19</sup> B. Y. Ber, Y. A. Kudriavtsev, A. V. Merkulov, S. V. Novikov, D. E. Lacklison, J. W. Orton, T. S. Cheng, and C. T. Foxon, *Semiconductor Science and Technology* **13**, 71 (1998).
  - <sup>20</sup> P. B. Shah, R. H. Dedhia, R. P. Tompkins, E. A. Viveiros, and K. A. Jones, *Solid-State Electronics* **78**, 121 (2012).
  - <sup>21</sup> H. J. von Bardeleben, J. L. Cantin, U. Gerstmann, A. Scholle, S. Greulich-Weber, E. Rauls, M. Landmann, W. G. Schmidt, A. Gentils, J. Botsoa, and M. F. Barthe, *Phys. Rev. Lett.* **109**, 206402 (2012).
  - <sup>22</sup> P. Hohenberg and W. Kohn, *Phys. Rev.* **136**, B864 (1964).
  - <sup>23</sup> W. Kohn and L. J. Sham, *Physical Review* **140** (1965).
  - <sup>24</sup> G. Henkelman, B. P. Uberuaga, and H. Jónsson, *Journal of Chemical Physics* **113**, 9901 (2000).
  - <sup>25</sup> G. Henkelman and H. Jónsson, *The Journal of Chemical Physics* **113**, 9978 (2000).
  - <sup>26</sup> G. Henkelman and H. Jónsson, *The Journal of Chemical Physics* **111**, 7010 (1999).
  - <sup>27</sup> M. G. Ganchenkova and R. M. Nieminen, *Phys. Rev. Lett.* **96**, 196402 (2006).
  - <sup>28</sup> K. H. Warnick, Y. Puzyrev, T. Roy, D. M. Fleetwood, R. D. Schrimpf, and S. T. Pantelides, *Phys. Rev. B* **84**, 214109 (2011).
  - <sup>29</sup> O. Ambacher, F. Freudenberg, R. Dimitrov, H. Angerer, and M. Stutzmann, *Japanese Journal of Applied Physics* **37**, 2416 (1998).
  - <sup>30</sup> K. H. Chow, G. D. Watkins, A. Usui, and M. Mizuta, *Phys. Rev. Lett.* **85**, 2761 (2000).
  - <sup>31</sup> P. Johannesen, A. Zakrzewski, L. S. Vlasenko, G. D. Watkins, A. Usui, H. Sunakawa, and M. Mizuta, *Phys. Rev. B* **69**, 045208 (2004).
  - <sup>32</sup> D. Sheppard and G. Henkelman, *J. Comput. Chem.* **32**, 1769 (2011).
  - <sup>33</sup> G. Kresse and J. Furthmüller, *Phys. Rev. B* **54**, 11169 (1996).
  - <sup>34</sup> P. E. Blöchl, *Phys. Rev. B* **50**, 17953 (1994).
  - <sup>35</sup> G. Kresse and D. Joubert, *Phys. Rev. B* **59**, 1758 (1999).
  - <sup>36</sup> J. P. Perdew, K. Burke, and M. Ernzerhof, *Phys. Rev. Lett.* **77**, 3865 (1996).
  - <sup>37</sup> J. Heyd, G. E. Scuseria, and M. Ernzerhof, *The Journal of Chemical Physics* **118**, 8207 (2003).
  - <sup>38</sup> J. Heyd, G. E. Scuseria, and M. Ernzerhof, *The Journal of Chemical Physics* **124**, (2006).
  - <sup>39</sup> The Transition State Tools implementation for VASP can be obtained from <http://theory.cm.utexas.edu/vtsttools>.
  - <sup>40</sup> C. Stampfl and C. G. Van de Walle, *Phys. Rev. B* **59**, 5521 (1999).
  - <sup>41</sup> M. Matsubara and E. Bellotti, arXiv:1507.06969 [cond-mat.mtrl-sci].
  - <sup>42</sup> S. Lany and A. Zunger, *Phys. Rev. B* **78**, 235104 (2008).
  - <sup>43</sup> C. Freysoldt, J. Neugebauer, and C. G. Van de Walle, *Phys. Rev. Lett.* **102**, 016402 (2009).
  - <sup>44</sup> S. B. Zhang, S.-H. Wei, and A. Zunger, *Phys. Rev. B* **63**, 075205 (2001).
  - <sup>45</sup> P. Erhart, A. Klein, and K. Albe, *Phys. Rev. B* **72**, 085213 (2005).
  - <sup>46</sup> H. Jónsson, G. Mills, and K. W. Jacobsen, in *Classical and Quantum Dynamics in Condensed Phase Simulations*, edited by B. J. Berne, G. Ciccotti, and D. F. Coker (World Scientific, 1998) Chap. 16, pp. 385–404.
  - <sup>47</sup> P. Erhart and K. Albe, *Phys. Rev. B* **73**, 115207 (2006).
  - <sup>48</sup> A. F. Wright, C. H. Seager, S. M. Myers, D. D. Koleske, and a. a. Allerman, *Journal of Applied Physics* **94**, 2311 (2003).
  - <sup>49</sup> C. G. Van de Walle, S. Limpijumnong, and J. Neugebauer, *Phys. Rev. B* **63**, 245205 (2001).
  - <sup>50</sup> U. Gerstmann, A. P. Seitsonen, and F. Mauri, *physica status solidi (b)* **245**, 924 (2008).
  - <sup>51</sup> K. H. Chow, G. D. Watkins, A. Usui, and M. Mizuta, *Physical Review Letters* **85**, 2761 (2000).
  - <sup>52</sup> R. Gillen and J. Robertson, *Journal of Physics: Condensed Matter* **25**, 405501 (2013).
  - <sup>53</sup> K. H. Chow, L. S. Vlasenko, P. Johannesen, C. Bozdog, G. D. Watkins, A. Usui, H. Sunakawa, C. Sasaoka, and M. Mizuta, *Phys. Rev. B* **69**, 045207 (2004).
  - <sup>54</sup> A. F. Wright, *Journal of Applied Physics* **92**, 2575 (2002).
  - <sup>55</sup> The charge deficiency is localized around the C–N<sub>3</sub> structure instead of just the carbon atom.
  - <sup>56</sup> W. Quapp, *Journal of Molecular Structure* **695-696**, 95 (2004).

- <sup>57</sup> V. Bakken, D. Danovich, S. Shaik, and H. B. Schlegel, *J. Am. Chem. Soc.* **123**, 130 (2001).
- <sup>58</sup> R. A. Swalin, in *Atomic Diffusion in Semiconductors*, edited by D. Shaw (Springer US, 1973) Chap. 2, pp. 65–110.
- <sup>59</sup> O. N. Bedoya-Martínez and G. Roma, *Phys. Rev. B* **82**, 134115 (2010).
- <sup>60</sup> A. F. Voter, in *Radiation Effects in Solids*, edited by K. E. Sickafus, E. A. Kotomin, and B. P. Uberuaga (Springer, 2007) Chap. 1, pp. 1–23.
- <sup>61</sup> M. Mantina, Y. Wang, R. Arroyave, L. Q. Chen, Z. K. Liu, and C. Wolverton, *Phys. Rev. Lett.* **100**, 215901 (2008).
- <sup>62</sup> A. Janotti and C. G. Van de Walle, *Phys. Rev. B* **76**, 165202 (2007).
- <sup>63</sup> J. D. Weeks, J. C. Tully, and L. C. Kimerling, *Phys. Rev. B* **12**, 3286 (1975).